



FACULTY OF MATHEMATICS AND NATURAL SCIENCES
UNIVERSITAS GADJAH MADA YOGYAKARTA

CERTIFICATE

This is to certify that:

Pranowo

has participated as a

PRESENTER

in The International Symposium on Computational Science (ISCS), conducted on May 15 - 16th, 2012 at the Faculty of Mathematics and Natural Sciences, Universitas Gadjah Mada.

Yogyakarta, May 16th, 2012

Organizing Committee ISCS

Faculty of Mathematics and Natural Sciences
Universitas Gadjah Mada



Dr. Chairil Anwar
Dean

Prof. Dr. Harno Dwi Pranowo, M.Sc.
Chairman

ISSN: 2252-7761

Computational Sciences and Applications

Volume 1:

**Proceeding of the Fifth
International Symposium
on Computational Science**

Yogyakarta, 15 – 16 May 2012

Editors:

Azhari

Pekik Nurwantoro

Ria Armunanto

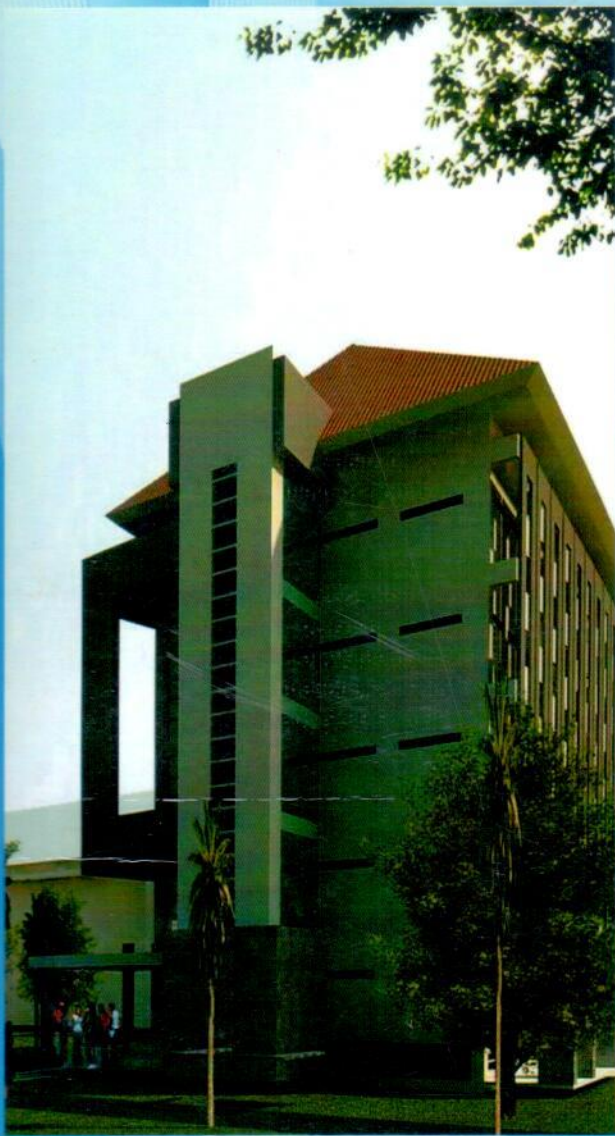
Ahmad Ashari

Danardono

Harno Dwi Pranowo

**FACULTY OF MATHEMATICS
AND NATURAL SCIENCES
UNIVERSITAS GADJAH MADA
YOGYAKARTA, INDONESIA**

2012



Center of Excellence in
Computational Science (COECS)
Faculty of Mathematics and
Natural Sciences,
Universitas Gadjah Mada



Department of Computational
Science, Faculty of Science,
Kanazawa University, Japan



Faculty of Mathematics and
Natural Sciences,
Institut Teknologi Bandung

ISSN: 2252-7761

COMPUTATIONAL SCIENCES AND
APPLICATIONS



Center of Excellence in
Computational Science (COECS)
Faculty of Mathematics and
Natural Sciences,
Universitas Gadjah Mada



Department of Computational
Science, Faculty of Science,
Kanazawa University, Japan



Faculty of Mathematics and
Natural Sciences,
Institut Teknologi Bandung

Volume 1:

Proceeding of the Fifth International Symposium on Computational Science

Yogyakarta, 15 – 16 May 2012

Editors:

Azhari

Pekik Nurwantoro

Ria Armunanto

Ahmad Ashari

Danardono

Harno Dwi Pranowo

FACULTY OF MATHEMATICS
AND NATURAL SCIENCES
UNIVERSITAS GADJAH MADA
YOGYAKARTA, INDONESIA

2012

LIST OF PAPERS

EIGEN FACE ALGORITHM FOR BATIK BOMBA RECOGNITION	1
Anita Ahmad Kasim, and Andi Hendra	1
SOFTWARE PARALLELIZATION FOR THE SIMULATION OF SOUND WAVES PROPAGATION WITH CUDA ARCHITECTURE.....	6
Arief Budiman, Pranowo, Yudi Dwi Andiyanta	6
UTILIZING 14 INDICATORS FOR FUJITSU'S STOCK USING FOURIER EXPANSION METHOD	14
Astrid Ayuningtyas	14
PARALLEL ALGORITHM DESIGN OF MOVING PARTICLE SEMI-IMPLICIT USING MESSAGE PASSING INTERFACE	22
Christian Fredy Naa, Suprijadi	22
SMOOTHED PARTICLE HYDRODYNAMICS METHOD FOR TWO-DIMENSIONAL STEFAN PROBLEM.....	34
Dede Tarwidi	34
STRUCTURAL, MAGNETIC AND ELECTRONIC PROPERTIES IN SMALL BISMUTH CLUSTERS Bi_N ($2 \leq N \leq 7$) ...	43
Ely Aprilia, Haruki Katou, Junpei Gotou, Shinya Haraguchi, Suprijadi, Tatsuki Oda	43
NUMERICAL SIMULATION OF DROPLET MOTION ON AN INCLINE PLANE	48
Elsa Pitriana	48
TRENDS AND CHALLENGES IN MOBILE COMPUTING DEVICES (SMARTPHONE)	57
Farindika Metandi and Azhari	57
NUMERICAL SIMULATION OF ORDER PARAMETER IN ANISOTROPIC SUPERCONDUCTOR	72
Fuad Anwar, Pekik Nurwantoro and Arief Hermanto	72
SOFTWARE DEVELOPMENT TOOL FOR IDENTIFICATION OF FINANCIAL MARKET INTERDEPENDENCE WITH GUMBEL-CLAYTON COPULA MODEL.....	81
Giovani Gracianti, Helena Margaretha, Sutrisno, Ronald Gunawan	81
OPTIMIZATION OF COLOUR REDUCTION FOR PRODUCING STEVIOSIDE SYRUP USING ANT COLONY ALGORITHM OF LOGISTIC FUNCTION	91
H.A Parhusip, and Yohanes Martono	91
NUMERICAL STUDY OF VORTEX DYNAMICS IN SQUID BASED ON THE MODIFIED TDGL EQUATIONS	102
Hari Wisodo, Pekik Nurwantoro, and Agung Bambang Setio Utomo.....	102
SPATIAL STATISTICAL ANALYSIS, MAPPING AND MODELING OF DENGUE HEMORRHAGIC FEVER IN BOGOR WEST JAVA INDONESIA.....	107
I Gede Nyoman Mindra Jaya, Budi Nurani Ruchjana, Atje Setiawan Abdullah, Toni Toharudin	107
PHASE TRANSITION PROBLEM SIMULATION WITH MOVING PARTICLE SEMI-IMPLICIT METHOD.....	125
Intan Hartri Putri	125
COMPUTATION FOR PRICING SHOUT OPTION.....	136
Irma Palupi	136
AN ONTOLOGY MODEL FOR ORGANIZING INFORMATION RESOURCES SHARING ON PERSONAL WEB ...	148
Istiadi and Azhari SN	148
A DFT-BASED COMPUTATIONAL STUDY ON HYDROGEN TUNNELING PHENOMENON IN THE ISOMERIZATION OF METHYLHYDROXYCARBENE.....	158
Jumaidil Awal, Rahmat Gunawan and Eva Marlina	158
THE DISCRETISATION OF AN INTEGRAL EQUATION FOR A SLUICE GATE FLOW	166
L.H. Wiryanto, Cyntia Paramitha, Zickry Zulkifti	166

GAMACLOUD-HPC: A PROPOSE MODEL FOR THE ARCHITECTURE OF COMPUTATIONAL SYSTEM BASED ON HIGH PERFORMANCE AND CLUSTER COMPUTING	173
Mardhani Riasetiawan	173
ANALYTICAL SOLUTION OF ATOMIC HYDROGEN BY ALGEBRAIC COMPUTATION	180
Moh Rosyid Mahmudi and Toto Winata	180
ANALYSIS OF A VIRUS DYNAMICS MODEL WITH MULTIPLE INFECTION	186
Nughthoh Arfawi Kurdhi	186
BLOOD COMPONENT CLASSIFICATION FOR MALARIA COMPUTER AIDED DIAGNOSIS FROM THIN BLOOD SMEAR MICROPHOTOGRAPHS.....	199
Nuke Dewi Kania, Theda Lukito, Anto Satriyo Nugroho, Ismail Ekoprayitno Rozi, Made Gunawan, Vitria Pragejsvara, Dian Anggraini	199
BASIS SET AND AB INITIO THEORY LEVEL OF RHODIUM(III)-WATER INTERACTION AS THE FIRST STEP OF QMCF MD SIMULATION	205
Ponco Iswanto, Eva Vaulina, Anung Riapanitra, Ria Armunanto, Harno Dwi Pranowo.....	205
NUMERICAL SIMULATION OF INTERACTION OF ULTRASONIC WAVE WITH BONE	211
Pranowo, Ratno Nuryadi.....	221
SOLUTION OF NANOMETER ORDER QUANTUM WELL BY COUPLED SCHRÖDINGER-POISSON EQUATIONS	229
Ratno Nuryadi	229
SOFT SOLUTION OF SOFT SET THEORY BASED ON AHP	234
RB. Fajriya Hakim and Dedi Rosadi.....	234
CONTENT-BASED IMAGE RETRIEVAL APPROACH FOR BATIK USING SHAPE FEATURES	248
Rima Tri Wahyuningrum and Fitri Damayanti.....	248
THE URANIUM BINDING SELECTIVITY OF 18-MEMBERED CROWN ETHERS: A DENSITY FUNCTIONAL STUDY.....	255
Saprizal Hadisaputra, Ria Armunanto and Harno D. Pranowo	255
SOLVING LOGICAL PUZZLES USING MATHEMATICAL MODELS	265
Susanti, Kie Van Ivanky Saputra, Samuel Lukas.....	265
RAINFALL FORECASTING FOR FLIGHT FEASIBILITY BASED ON ADAPTIVE NEURO FUZZY INFERENCE SYSTEMS	277
Sungging Haryo W., Syamsul Arifin, Iftikar Luthfi, Asthy Farida	277
APPLICATIONS OF NUMERICAL SIMULATION ON COASTAL MORPHOLOGICAL DYNAMIC STUDIES	285
Syamsidik, Arizal, and Shinta Dewi.....	285
SEMI-AUTOMATED COMPUTER-AIDED DIAGNOSIS FOR MALARIA MULTI SPECIES PARASITE DETECTION FROM THIN BLOOD SMEAR MICROPHOTOGRAPHS	296
Theda Lukito, Nuke Dewi Kania, Ismail Ekoprayitno Rozi, Anto Satriyo Nugroho, Made Gunawan, Vitria Pragejsvara, Dian Anggraini.....	296
3D HOLOGRAPHIC DISPLAY FOR THE FUTURE TECHNOLOGY	303
Vivie Deyby Kumenap and Azhari	303

NUMERICAL SIMULATION OF INTERACTION OF ULTRASONIC WAVE WITH BONE

Pranowo

Teknik Informatika Universitas Atma Jaya Yogyakarta
Jl. Babarsari 43 Yogyakarta 55281 Indonesia

Email: pran@staff.uajy.ac.id

Abstract. Better understanding of the mechanism in which ultrasonic wave interacts with bone is important in therapy and diagnosis alike, such as extracorporeal shock wave therapy (ESWT). In this paper, numerical simulation for investigating the interaction of ultrasonic wave with bone is presented. The elastodynamic equations was used as the governing equations. A nodal high order discontinuous galerkin finite element was used for the spatial discretization while an explicit low storage fourth order Runge Kutta scheme is used to march in the time domain. This paper demonstrated the power of numerical method for biomedical research, which deals with ultrasonic wave propagation in human body.

Keywords: ultrasonic wave, bone, discontinuous galerkin

1. INTRODUCTION

Interaction between ultrasonic wave propagation with bone occurs in many biomedical treatments, such as extracorporeal shock wave therapy (ESWT). The ESWT is a noninvasive treatment for a variety of musculoskeletal ailments. The ultrasonic shock wave is generated by a spark plug source (lithotripter) in water and then focused using an acoustic lens or reflector so the energy of the wave is concentrated in a small treatment region (Fagnan, 2010).

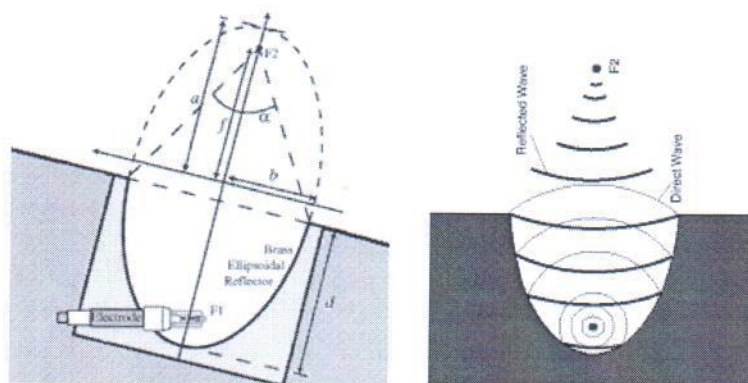


Figure1. Lithotripter

Better understanding of the mechanism of the interaction of the ultrasonic wave with bone is important for the biomedical treatment. In this paper, numerical simulation approach for investigating the mechanism was proposed.. The bone was assumed as elastic solid material and the water as inviscid fluid. The water can be treated as solid with zero shear stress. Therefore a single partial differential equation system, called elastodynamics equations, can be applied as the governing equations for both materials. Then the governing equations is formulated in terms of velocity-stress in both media.

Many numerical method were proposed for the solution of the governing equations [e.g. finite difference time domain (FDTD) or finite element methods (FEM)]. The FDTD method (Kaufmann et al., 2008; Matsukawa et al., 2008) is limited for simple spatial domain only and the conventional FEM (Protopappas et al., 2007; Nguyen et al., 2010) has a high dispersion error. A nodal high order discontinuous galerkin (DG) finite element is used for the spatial discretization while an explicit low storage fourth order Runge Kutta scheme is used to march in the time domain. The DG method can applied for irregular domain and has low dispersion error.

The simulation of ultrasonic wave by discontinuous galerkin method in unbounded domains requires a specific boundary condition of the necessarily truncated computational domain. We propose an absorbing boundary condition called perfectly matched layer (PML). Presented in time domain electromagnetic simulations (Berenger, 1996), PML has since been used extensively in that field. PML has also been incorporated into a variety of wave propagation algorithms. Colino and Tsogka (2001) have formulated and demonstrated PML in the P-SV case via Virieux (1986) finite difference scheme and a mixed finite element algorithms.

2. GOVERNING EQUATIONS

Starting with the system of governing equations, each equation is split into a parallel and perpendicular component, based on spatial derivative separation. That is, the perpendicular equations contains the spatial derivative term which acts normal to the coordinate plane of interest and a damping term, and the parallel equation contain the remaining spatial derivative terms. Finally, an additional equation is required to sum the results of the split equations

$$\begin{aligned}
 \frac{\partial v_{xx}}{\partial t} + \sigma(x)v_{xx} &= \frac{1}{\rho} \frac{\partial \tau_{xx}}{\partial x} + f_x & ; & \quad \frac{\partial v_{xy}}{\partial t} + \sigma(y)v_{xy} = \frac{1}{\rho} \frac{\partial \tau_{xy}}{\partial y} \\
 \frac{\partial v_{yx}}{\partial t} + \sigma(x)v_{yx} &= \frac{1}{\rho} \frac{\partial \tau_{xy}}{\partial x} & ; & \quad \frac{\partial v_{yy}}{\partial t} + \sigma(y)v_{yy} = \frac{1}{\rho} \frac{\partial \tau_{yy}}{\partial y} + f_y \\
 \frac{\partial \tau_{xxx}}{\partial t} + \sigma(x)\tau_{xxx} &= (\lambda + 2\mu) \frac{\partial v_x}{\partial x} & ; & \quad \frac{\partial \tau_{xxy}}{\partial t} + \sigma(y)\tau_{xxy} = \lambda \frac{\partial v_y}{\partial y} \\
 \frac{\partial \tau_{yyx}}{\partial t} + \sigma(x)\tau_{yyx} &= \lambda \frac{\partial v_x}{\partial x} & ; & \quad \frac{\partial \tau_{yyy}}{\partial t} + \sigma(y)\tau_{yyy} = (\lambda + 2\mu) \frac{\partial v_y}{\partial y} \\
 \frac{\partial \tau_{xyx}}{\partial t} + \sigma(x)v_{xyx} &= \mu \frac{\partial v_y}{\partial x} & ; & \quad \frac{\partial \tau_{xyy}}{\partial t} + \sigma(y)v_{xyy} = \mu \frac{\partial v_x}{\partial y}
 \end{aligned}
 \tag{1}$$

$$v_x = v_{xx} + v_{xy}, \quad v_y = v_{yx} + v_{yy}, \quad \tau_{xx} = \tau_{xxx} + \tau_{xxy}, \quad \tau_{yy} = \tau_{yyx} + \tau_{yyy}, \quad \tau_{xy} = \tau_{xyx} + \tau_{xyy}$$

In the absorbing layers we use the following model for the damping parameters:

$$\sigma(x) = d_0 \left(\frac{x}{\delta} \right)^2 \quad ; \quad \sigma(y) = d_0 \left(\frac{y}{\delta} \right)^2 \quad \text{and} \quad d_0 = \log \left(\frac{1}{R} \right) \frac{3c_p}{2\chi}$$

where δ is the length of the layer and d_0 is a function of the theoretical reflection coefficient (R)

3. DISCONTINUOUS GALERKIN METHOD

For simplicity, the split equations (2) are written in vector form as follows:

$$\frac{\partial \mathbf{q}}{\partial t} + \mathbf{A} \frac{\partial \mathbf{q}}{\partial x} + \mathbf{B} \frac{\partial \mathbf{q}}{\partial y} = \mathbf{f} \quad (2)$$

where $\mathbf{q} = [v_{xx} \ v_{xy} \ v_{yx} \ v_{yy} \ \tau_{xxx} \ \tau_{xxy} \ \tau_{yyx} \ \tau_{yyy} \ \tau_{xyx} \ \tau_{xyy}]^T$

The spatial derivatives are discretized by using a discontinuous galerkin method. The simplified of Eq.(2) according to Galerkin's procedure using the same basis function ϕ within each element is defined below (Hesthaven & Warburton, 2002; 2008).

$$\begin{aligned} \left(\phi, \frac{\partial \mathbf{q}}{\partial t} + \mathbf{A} \frac{\partial \mathbf{q}}{\partial x} + \mathbf{B} \frac{\partial \mathbf{q}}{\partial y} \right) &= 0 \\ \Leftrightarrow \left(\phi, \frac{\partial \mathbf{q}}{\partial t} \right)_{\Omega} + \left(\phi, \mathbf{A} n_x \mathbf{q} + \mathbf{B} n_y \mathbf{q} \right)_{\partial \Omega} - \left(\frac{\partial}{\partial x} (\mathbf{A} \phi), \mathbf{q} \right)_{\partial \Omega} - \left(\frac{\partial}{\partial y} (\mathbf{B} \phi), \mathbf{q} \right)_{\partial \Omega} &= 0 \end{aligned} \quad (3)$$

Here (...) represents the normal 2 L inner product, the second term is flux vector and (n_x, n_y) are normal vector. The mathematical manipulation of the flux vector is calculated as below:

$$\left(\phi, \frac{\partial \mathbf{q}}{\partial t} + \mathbf{A} \frac{\partial \mathbf{q}}{\partial x} + \mathbf{B} \frac{\partial \mathbf{q}}{\partial y} \right)_{\Omega} + \left(\phi, \mathbf{A} n_x + \mathbf{B} n_y \right) (\bar{\mathbf{q}} - \mathbf{q}^-)_{\partial \Omega} = 0 \quad (5)$$

where $\mathbf{q}^-|_{\partial \Omega} = \hat{\mathbf{q}}^- (\mathbf{q}^-, \mathbf{q}^+)$ and the last term of equation (3) is called numerical flux.

Here, we took the Kornwinder Dubiner function on straight sided triangle as the basis written in equation 4 (see Figs. 1 and 2):

$$\phi_{ij}(r, s) = \sqrt{\frac{2i+1}{2}} \sqrt{\frac{2i+2j+2}{2}} P_i^{0,0} \left(\frac{2(1+r)}{(1-s)} - 1 \right) P_j^{2=+1,0}(s) \quad (4)$$

where, $P^{\alpha,\beta}$ is orthogonal Jacobi polynomial

All straight sided triangles are the image of this triangle under the map:

$$\begin{pmatrix} x \\ y \end{pmatrix} = -\left(\frac{r+s}{2} \right) \begin{pmatrix} v_x^1 \\ v_y^1 \end{pmatrix} + \left(\frac{1+r}{2} \right) \begin{pmatrix} v_x^2 \\ v_y^2 \end{pmatrix} + \left(\frac{1+s}{2} \right) \begin{pmatrix} v_x^3 \\ v_y^3 \end{pmatrix} \quad (5)$$

The set of points in the triangle, which we can build the Lagrange interpolating polynomials, can be viewed as Gauss-Legendre -Lobatto (GLL) points.

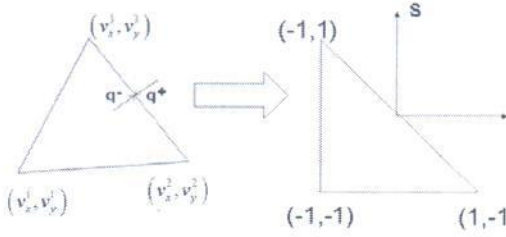


Figure 2: Coordinate Transformation

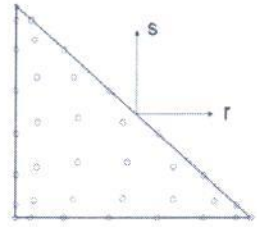


Figure 3: Seventh Order Gauss Lobatto Quadrature Nodes

The vector \mathbf{q} is expanded using equation (4), we take expansion of v_x as example:

$$v_x(r, s) = \sum_{i=0}^N \sum_{j=0}^{N-i} \phi_{ij}(r, s) \widehat{v}_{xij} \tag{6}$$

$$v_x(r_n, s_n) = \sum_{m=1}^{m=M} \mathbf{V}_{nm} \widehat{v}_{xm} \tag{7}$$

$$\widehat{v}_{xm} = \sum_{j=1}^{m=M} (\mathbf{V}^{-1})_{mj} v_x(r_j, s_j)$$

$$\begin{aligned} \frac{\partial v_x}{\partial r}(r, s) &= \sum_{i=0}^N \sum_{j=0}^{N-i} \frac{\partial \phi_{ij}}{\partial r}(r, s) \widehat{v}_{xij} = \widehat{\mathbf{D}}^r \mathbf{V}^{-1} v_x(r, s) & \widehat{\mathbf{D}}^r &= \frac{\partial \phi}{\partial r} \\ \frac{\partial v_x}{\partial s}(r, s) &= \sum_{i=0}^N \sum_{j=0}^{N-i} \frac{\partial \phi_{ij}}{\partial s}(r, s) \widehat{v}_{xij} = \widehat{\mathbf{D}}^s \mathbf{V}^{-1} v_x(r, s) & \widehat{\mathbf{D}}^s &= \frac{\partial \phi}{\partial s} \end{aligned}$$

where \mathbf{V}_{ij} and N are Vandermonde matrix and the order of Jacobi polynomial respectively.

The semi discrete Eq. (3) is integrated in time marching by using five stage of fourth order 2N-storage Runge-Kutta scheme as developed by Carpenter & Kennedy (1994). The final equations are found as written in Eq. (8).

$$\begin{aligned} \frac{d\mathbf{q}}{dt} &= L[t, \mathbf{q}(t)] & (8) \\ d\mathbf{q}_j &= A_j d\mathbf{q}_{j-1} + dt L(\mathbf{q}_j) \\ \mathbf{q}_j &= \mathbf{q}_{j-1} + B_j + d\mathbf{q}_j \end{aligned}$$

where dt is the time step. The vectors A and B are the coefficients that will be used to determine the properties of the scheme. The maximum time step is (Hesthaven and Warburton, 2002):

$$\Delta t \leq \frac{2h}{c_p(N-1)^2} \tag{9}$$

where c_p is primary wave velocity and h is the smallest edge length of the element

4. RESULTS AND DISCUSSIONS

In this section we present two numerical examples. The the first example aims at showing the accuracy of DGM compared to analytical solution and Fem whis proposed by Diaz and Patrick (2005) and the second example aims at showing that DGM can easily handle problems with complicated interface.

4.1 Numerical Example I

The first example has a simple configuration: two half-planes separated by a straight interface, one constitutes the fluid medium and the second one constitutes solid medium. The material properties for the fluid are $c_p = 1500 \text{ ms}^{-1}$, $c_s = 0 \text{ ms}^{-1}$ and $\rho = 1000 \text{ kg m}^{-3}$ and the material properties for the solid are $c_p = 4000 \text{ ms}^{-1}$, $c_s = 1800 \text{ ms}^{-1}$ and $\rho = 1850 \text{ kg m}^{-3}$. The size of each medium is $20 \text{ mm} \times 5 \text{ mm}$. We added absorbing layer surrounding the domain with the thickness of the layer equals 1 mm and total number of triangular elements is 15060. The polynomial degree is $N=3$ and the time step $\Delta t = 10^{-8} \text{ s}$. The source function is a point source located in the fluid at 2 mm above the interface, the time variation of the source is given as Gaussian with dominating frequency is 1 MHz Snapshots of the first example can be seen in figure 4a - 4b.

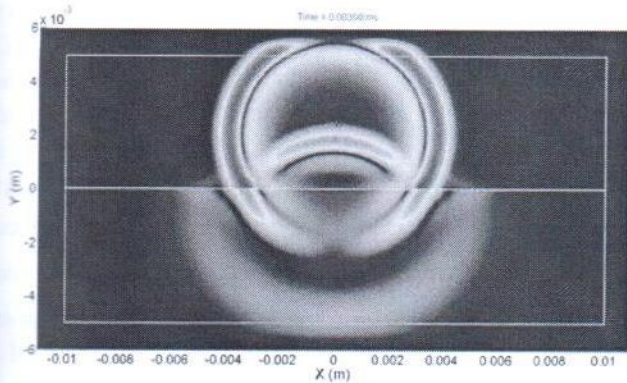


Figure 4a: Velocity fields of 1st example at $0.36 \mu\text{s}$

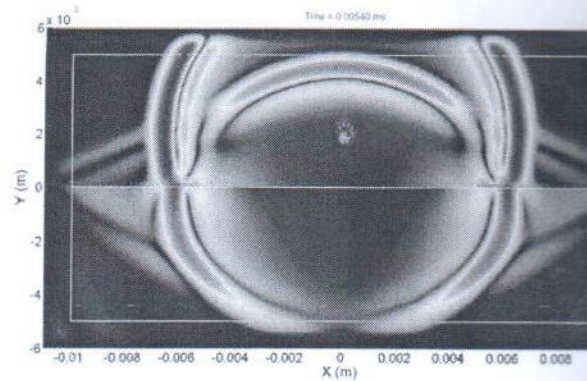
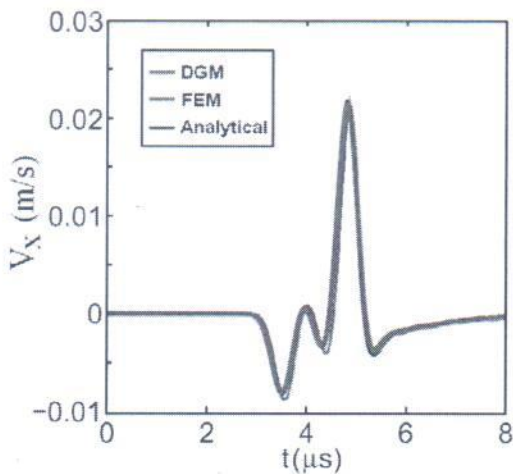
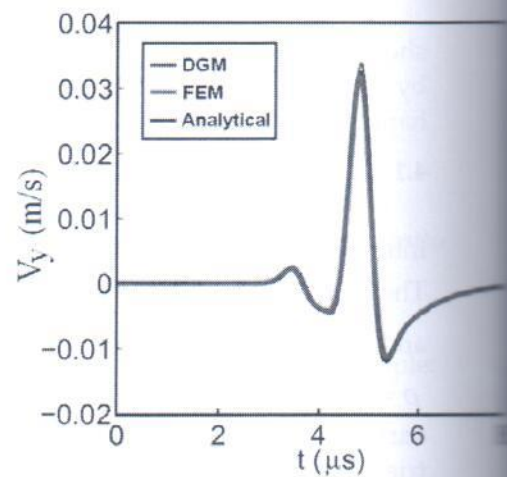


Figure 4b: Velocity fields of 1st example at $0.54 \mu\text{s}$

To validate the DG method, we compare the numerical DGM (the green curve) solution to the FEM solution (the red curve) and analytical solution (the blue curve) which are provided by Diaz and Patrick. (2005). the two components of the numerical and analytical velocity are shown by figure 5a and 5b. The curves are perfectly superimposed, showing the good accuracy of DGM. From 4b we can see no reflection on the left, right and bottom edges. The PML absorbed the outgoing waves well.

Figure 5a: Horizontal velocity (v_x)Figure 5b: Vertical velocity (v_y)

4.2 Numerical Example II

In this example, the interaction of ultrasonic wave propagation, which generated by lithotripter, with human skull. The contour of human skull was extracted from MRI scanned image by using level set segmentation, as shown in figure 6. Figure 7 shown the whole of physical domain, including lithotripter and absorbing layer. The major and minor axes of the ellipsoid of the lithotripter are $a = 70$ mm and $b = 40$ mm. The domain is discretized into triangular 7433 elements. The material properties for the water are $\mu = 0$ GPa, $\lambda = 2.2$ GPa and $\rho = 1000$ kg m⁻³ and the material properties for the bone are $\mu = 9.4$ GPa, $\lambda = 20$ GPa and $\rho = 2000$ kg m⁻³. The polynomial degree is $N = 4$ and the time step $\Delta t = 10^{-8}$ s. The source function is a point source located at the focus of ellipsoid, the time variation of the source is given as Ricker (i.e., the first derivative of a Gaussian) with dominating frequency is 0.5 MHz

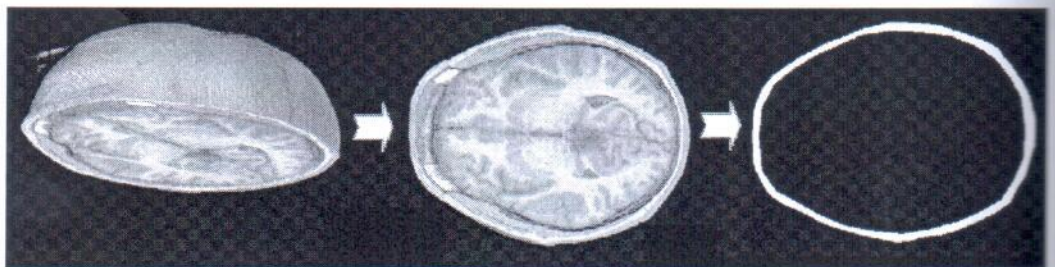


Figure 6. Horizontal section of human head and the bone segmentation
https://www.msu.edu/~brains/brains/human/horizontal/1400_cut.html

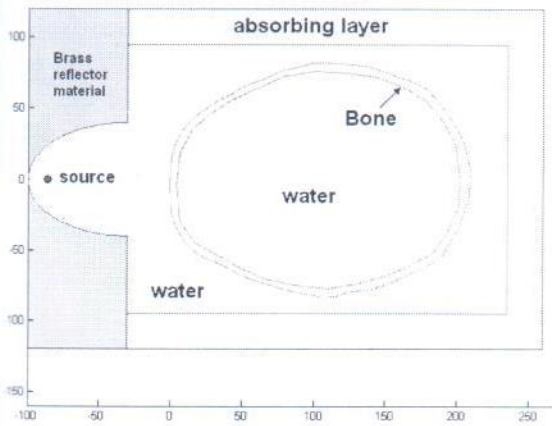


Figure 7. The domain of the 2nd example

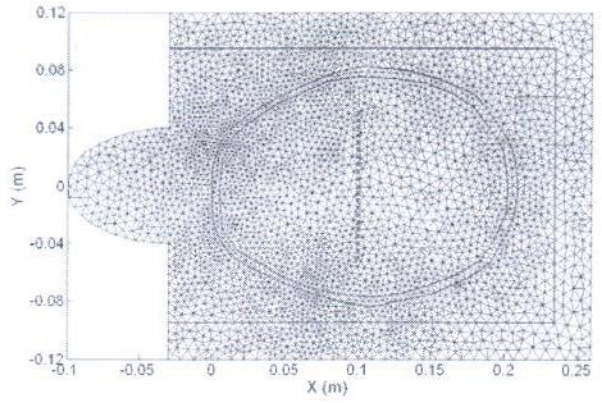


Figure 8. Mesh of the 2nd example, red crosses

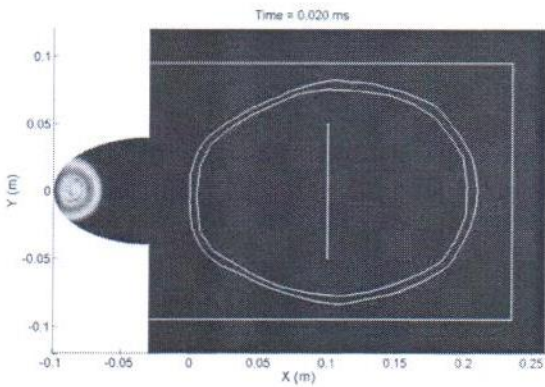


Figure 9a: Velocity fields of 2nd example at 20 μ s

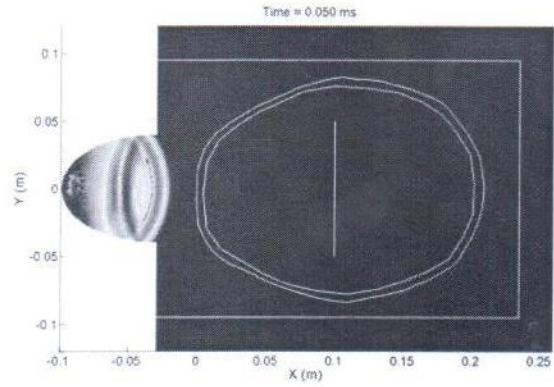


Figure 9b: Velocity fields of 2nd example at 50 μ s

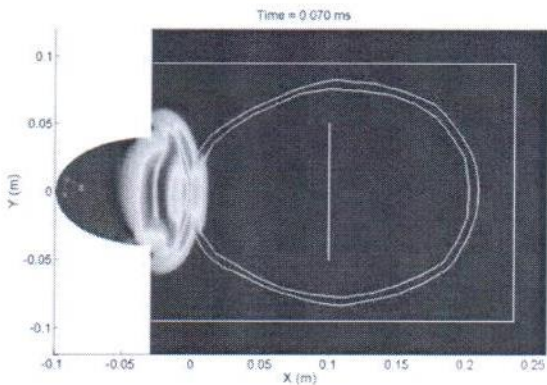


Figure 9c: Velocity fields of 2nd example at 70 μ s

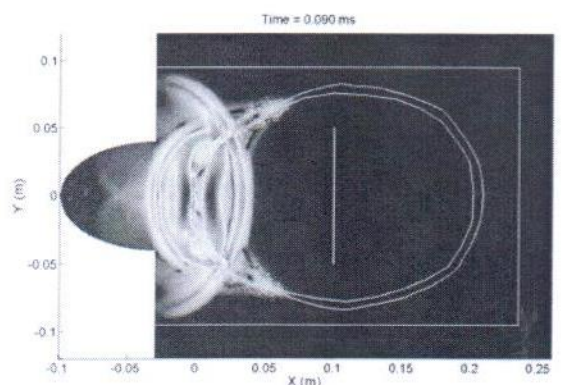


Figure 9d: Velocity fields of 2nd example at 090 μ s

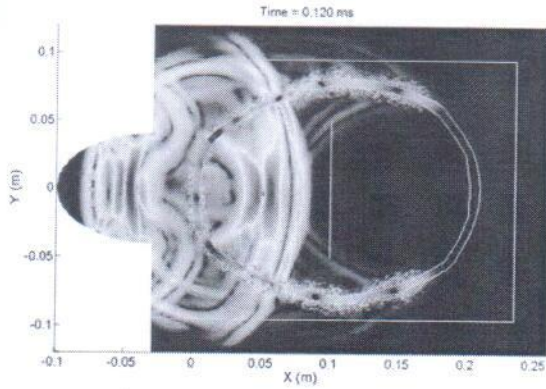


Figure 9e: Velocity fields of 2nd example at 120 μ s

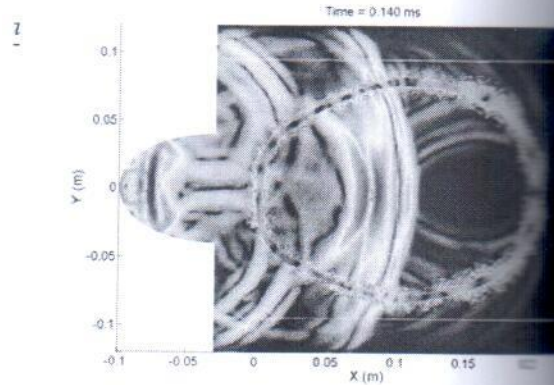


Figure 9f: Velocity fields of 2nd example at 140 μ s

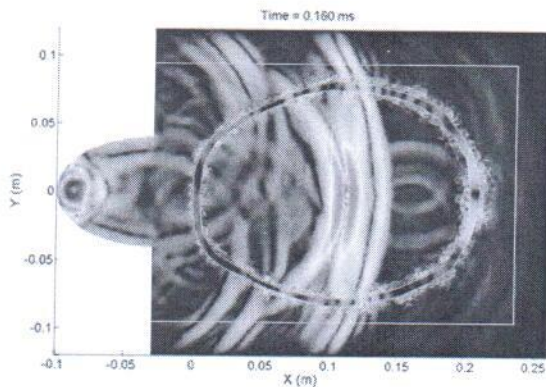


Figure 9g: Velocity fields of 2nd example at 160 μ s

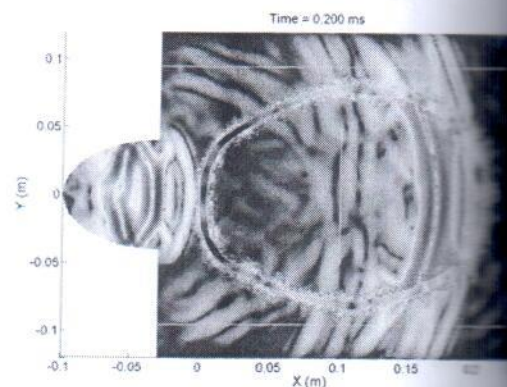


Figure 9h: Velocity fields of 2nd example at 200 μ s

Figure 10.a and 10.b contain the traces recorded at receiver position = (0.1, 0.05), and figure 10.c contains the traces recorded at all receiver position. As one can see from the figure, the solutions obtained from discontinuous galerkin methods has smooth solution contained no numerical oscillation.

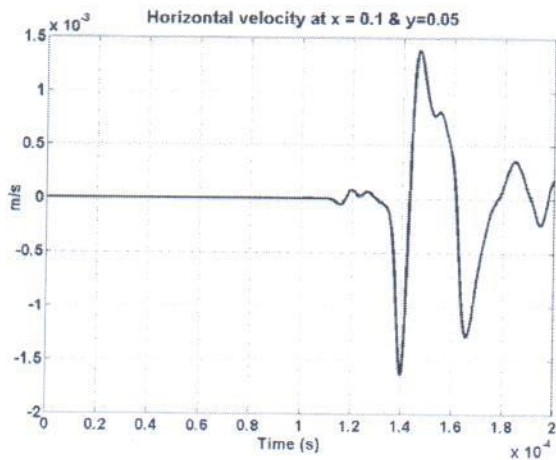


Figure 10a: Horizontal velocity (v_x) recorded at receiver position $x = 0.1$ and $y = 0.05$ m

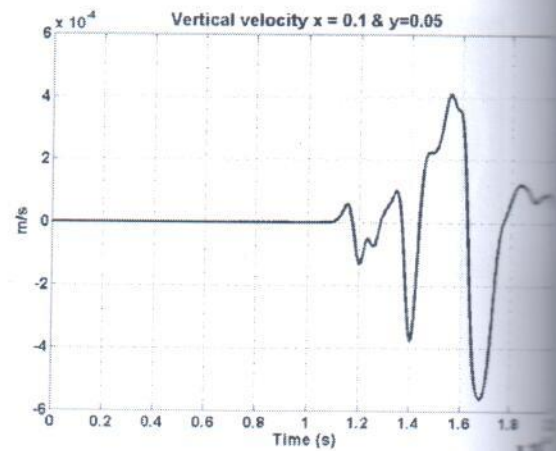


Figure 10b: Vertical velocity (v_y) at receiver position $x = 0.1$ and $y = 0.05$ m

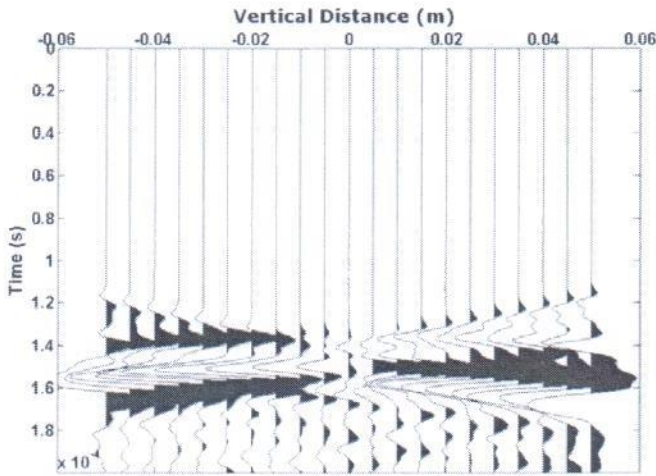


Figure 11: Vertical velocity (v_x) at all receiver positions $x=0.1$ and $y=-0.05$ through $z=0.05$ m

5. CONCLUSIONS

In this paper, numerical simulation for investigating the interaction of ultrasonic wave with bone based on discontinuous galerkin method is presented. To model the interaction ultrasonic wave with bone, bone material was considered as a elastic solid medium immersed in an acoustic fluid. The discontinuous galerkin method provides stable and accurate methods for simulating the interaction ultrasonic wave with bone. It is shown that numerical simulation is a valuable tool for investigating ultrasonic wave interactions with bone. Numerical simulation can provide important insights that can lead to many practical advantages, dealing with ultrasonic wave propagation in human body.

REFERENCES

- Berenger, J. P. (1996). Three-Dimensional Perfectly Matched Layer for the Absorption of Electromagnetic Waves. *Journal Computational Physics*, 127, pp. 1363-379.
- Carpenter, M. H.; and Kennedy, C. A. (1994). Fourth-order 2N-Storage Runge-Kutta Schemes. NASA Technical Memorandum 109112, NASA Langley Research Center, Hampton, Virginia.
- Collino, F.; and Tsogka, C. (2001). Application of the PML absorbing layer model to the linear elastodynamic problem in anisotropic heterogeneous medium. *Geophysical Journal International*, Vol. 66, No. 1, pp. 294-307, 2001
- Diaz, J.; and Patrick, J. (2005). Robust high order non-conforming finite element formulation for time domain fluid-structure interaction. *Journal of Computational Acoustics*, World Scientific, 13 (3), pp. 403-431.
- Fagnan, K. M.. (2010). High-resolution Finite Volume Methods for Extracorporeal Shock Wave Therapy. Ph.D. Thesis. University of Washington.
- Hesthaven, J. S.; and Warburton, T. (2002). High-order Nodal Methods on Unstructured Grids, I. Time Domain Solution of Maxwell's Equation. *J. Computational Physics*, 181, pp. 1-34.
- Hesthaven, J. S.; and Warburton, T. (2008). *Nodal Discontinuous Galerkin Methods: Algorithms, Analysis, and Applications*, Springer, New York.

- Kaufman, J.J., Gangming, L., and Siffert, R. S. (2008). Ultrasound Simulation in Bone. *IEEE Transactions on Ultrasonics, Ferroelectrics, And Frequency Control*, Vol. 55, No. 6, June 2008
- Matsukawa, M., Mizuno, K., and Nagata, Y. (2008). The fast wave propagation in bovine cancellous bone-experiments and simulation. *The European Acoustics Association Conference*, June 29-July 4, 2008, Paris, France.
- Nguyen, V. H., Naili, S., and Sansalone, V. (2010). Simulation of ultrasonic wave propagation in anisotropic cancellous bone immersed in fluid. *Wave Motion*, Volume 47, Issue 2, March 2010. Pages 117-129.
- Protopappas, V.C. et al. (2007). Three-dimensional finite element modeling of guided ultrasonic wave propagation in intact and healing long bones. *J. Acoust. Soc. Am.* 121 (6) June 2007.